Estimation of Velocity from Argos-tracked Surface Drifters during OCEAN STORMS

ERIC A. D'ASARO

Applied Physics Laboratory and School of Oceanography, College of Ocean and Fishery Sciences, University of Washington, Seattle, Washington

23 September 1991 and 17 December 1991

ABSTRACT

Modern surface drifters tracked by Argos are an attractive method for measuring the spatial structure of near-surface currents. This note discusses the accuracy to which velocity can be estimated from such data, assuming perfect drifters. The analysis concentrates on data from OCEAN STORMS centered at 47.5°N in the eastern North Pacific, a region of low mesoscale activity. The irregular, but nearly diurnally repeating, pattern of fixes leads to leakage between near-inertial (1.48 cpd) and subinertial (0.5 cpd) frequencies. Total spectral leakage for a naive spline interpolant of the fixes is about 2×10^{-3} in energy, or 5% in amplitude. Other interpolants can produce an order of magnitude more leakage. An algorithm that controls these errors is described. Only an inertial peak and frequencies well below 0.5 cpd can be resolved. The remaining noise can be described as the sum of a random fix error of 600 m rms and unresolved subinertial velocities with an rms displacement of about 550 m. The errors in the computed inertial and low-frequency velocities are 0.03 and 0.01 m s^{-1}, respectively. These can be reduced with further time averaging. Significantly better estimates of velocities would require both more accurate and more frequent position fixes.

1. Introduction

Modern surface drifters tracked by the Argos satellite tracking system offer an inexpensive way to measure near-surface current with an accuracy approaching that of moored current meters (Chereskin et al. 1989). Deployed in large arrays, they offer an unmatched capability to map the two-dimensional field of near-surface currents over long periods of time. This capability is limited at high frequencies by the characteristics of Service Argos, as is explored in this note.

Forty-nine TRISTAR-II (Niiler et al. 1987) drifters were deployed in a coherent array about 250 km across near 147.5°N, 140°W as part of the OCEAN STORMS experiment in October 1987. Position data for these drifters were provided by Service Argos. The goal of this array was to map the near-inertial and low-frequency currents, particularly those generated by the strong winter storms in this area. This note estimates the errors in near-inertial and low-frequency currents estimated from these buoys due to random and sampling errors inherent in Service Argos. Chereskin et al. (1989) provide estimates of the errors due to buoy slippage.

Corresponding author address: Dr. Eric A. D'Asaro, University of Washington, Applied Physics Laboratory, 1013 N.E. 40th St., Seattle, WA 98105-6698.

2. Sources of error in Argos tracking

An obvious source of error in velocities computed from Argos-tracked drifters is the random error in the fixes. Service Argos quotes rms errors less than 350 m in each component for fix "qualities" 2 and 3 used here. For moving drifters, additional nearly random error will be contributed by unresolved high-frequency motions induced by surface and internal gravity waves.

More subtle aliasing errors result from the temporal sampling pattern. Argos fixes arrive in an irregular pattern, which nearly repeats with a period of one solar day. For the case shown in Fig. 1, which is representative of OCEAN STORMS, a data gap about 10 h long occurs each day, during which a single fix or none arrives. Since there is little information during these gaps, energy with periods 10 h or shorter will be aliased. Errors also occur for subinertial frequencies. At 47.5°N, three inertial periods equal about 2 days (3×16.3 h = 48.9 h). For a pure inertial signal this implies alternating positive and negative maxima during the data gap (Fig. 1, top) on successive days. A sinusoidal signal with a period near 2 days produces a similar signal (Fig. 1, bottom). These frequencies cannot be distinguished independently by the Argos sampling pattern.

Figure 2 demonstrates these effects. One simple way to compute a velocity from irregularly spaced position data is to interpolate and differentiate the positions with a cubic spline. The velocity spectrum of a perfect

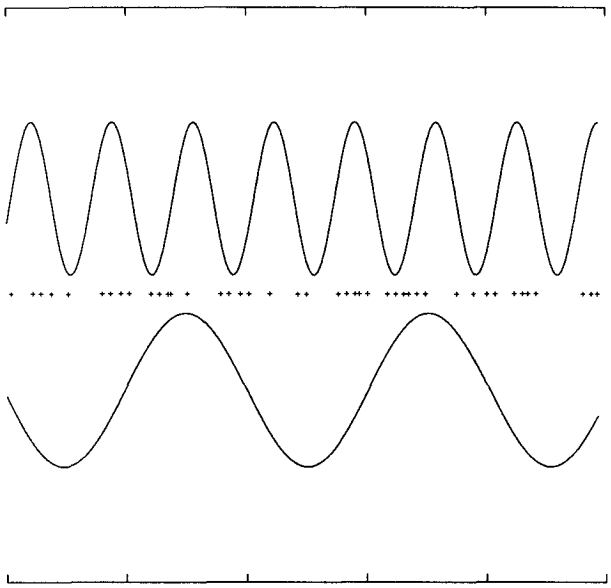

FIG. 1. Argos sampling times (+) for buoy 7944 starting on day 275 of 1987. Ticks mark 1-day intervals. Sinusoidal curves with inertial (top) and 2-day (bottom) period are affected by the daily data gaps in a similar way leading to spectral leakage.

inertial oscillation, sampled at hourly intervals for 256 h, shows a peak at the inertial frequency with no sidelobes (Fig. 2, heavy line). The same signal, sampled at the Argos fix times for OCEAN STORMS buoy 7944 from day 278 to 296.3 of 1987, has a spectrum (Fig. 2, light line) with significant leakage to both superinertial and subinertial frequencies and a peak at 0.5 cpd. The total leakage energy is about 2% of the input inertial energy; the subinertial part is about 2×10^{-3}. For 0.3 m s^{-1} inertial currents, which are common in these data, this implies contamination of subinertial velocities of about 0.01 m s^{-1}. This is significant compared with both the low-frequency velocities and the spatial variations in the demodulated inertial currents. Other demodulation schemes can lead to much larger leakage, as will be seen.

3. Analysis methods

The leakage shown in Fig. 2 can be controlled by filtering the spectral content of the desired "signal" and leaving as "noise" those frequencies that cannot be properly resolved. Because the 10-h gaps in Argos sampling suggest that the lowest frequency that can be unambiguously resolved is close to the inertial, we do not try to resolve frequencies higher than that. The coupling of inertial and 0.5-cpd frequencies suggests that only frequencies less than 0.5 cpd can be unambiguously resolved, so we extract a signal only with inertial and less than 0.5 cpd (here called "low frequency") components. Other frequencies will be mostly noise. Furthermore, only temporal variations of the inertial component with frequencies less than 0.5 cpd can be resolved.

The following algorithm was used. The position of a buoy will be specified by its east (x) and north (y) displacements as a complex number

$$X = x + iy, \tag{1}$$

which is a continuous function of time t. This is modeled as the sum of low-frequency (subscript L) and near-inertial (subscript I) components and a random noise component ϵ:

$$X(t) = X_L(t) + \tilde{X}_I(t)e^{-ift} + \epsilon(t), \tag{2}$$

where f is the inertial frequency at a fixed reference latitude (here 47.5°N), and X_L and $\tilde{X}_I$ are assumed to vary slowly compared with f^{-1}.

Using a fixed f causes the slow changes in f due to the drifter's motion to show up as changes in the phase of the inertial currents, so that the pattern of inertial phases from a buoy array will correctly represent the spatial pattern of currents at a fixed time. In contrast, using a time variable f (Poulain 1990) hides this structure within the demodulation. The pattern of demodulated currents does not represent a true spatial current pattern in this case.

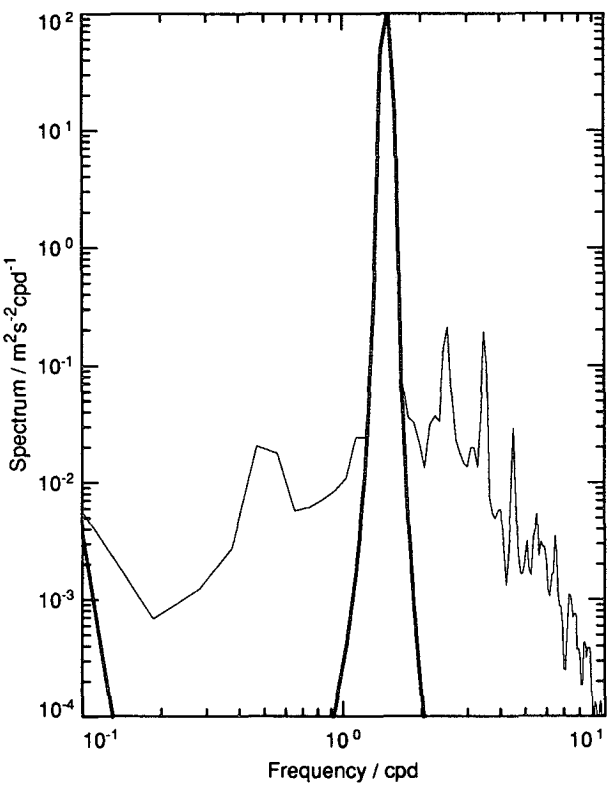

FIG. 2. Spectrum of a pure inertial oscillation sampled at hourly intervals (heavy curve) and sampled at the Argos fix times and interpolated with a cubic spline (light curve). Note the additional spectral leakage.

Filtering of irregularly spaced data is conveniently done using smoothing splines (Craven and Wahba 1979). Given a vector of input data $\mathbf{X}^*$ sampled at times $\mathbf{t}^*$ and a smoothing parameter T_S, these produce a continuous smooth function $S(\mathbf{X}^*, \mathbf{t}^*, T_S; t)$. For equally spaced data, cubic smoothing splines are equivalent to the product of two low-pass Butterworth filters such that the amplitude is reduced by a factor of 2 at a wavelength $2\pi T_S$ (Craven and Wahba 1979).

An initial estimate of X_L is computed as

$$X_{L1}(t) = S(\mathbf{X}^*, \mathbf{t}^*, T_L; t). \quad (3)$$

The smoothing parameter T_L sets the frequency that separates low-frequency motions from inertial motions and noise. The demodulated inertial component is then computed:

$$\tilde{X}_I(t) = S\{[\mathbf{X}^* - \mathbf{X}_{L1}(\mathbf{t}^*)] \cdot \mathbf{e}^{if\mathbf{t}^*}, \mathbf{t}^*, T_I; t\}, \quad (4)$$

where $\mathbf{X}_{L1}(\mathbf{t}^*)$ and $\mathbf{e}^{if\mathbf{t}^*}$ denote the vectors produced by sampling $X_{L1}(t)$ and $e^{if t}$ at times $\mathbf{t}^*$. The inertial frequency displacements are

$$X_I(t) = \tilde{X}_I(t)e^{-if t}. \quad (5)$$

The smoothing parameter T_I sets the bandwidth of the inertial peak. A final estimate of the low-frequency motions is

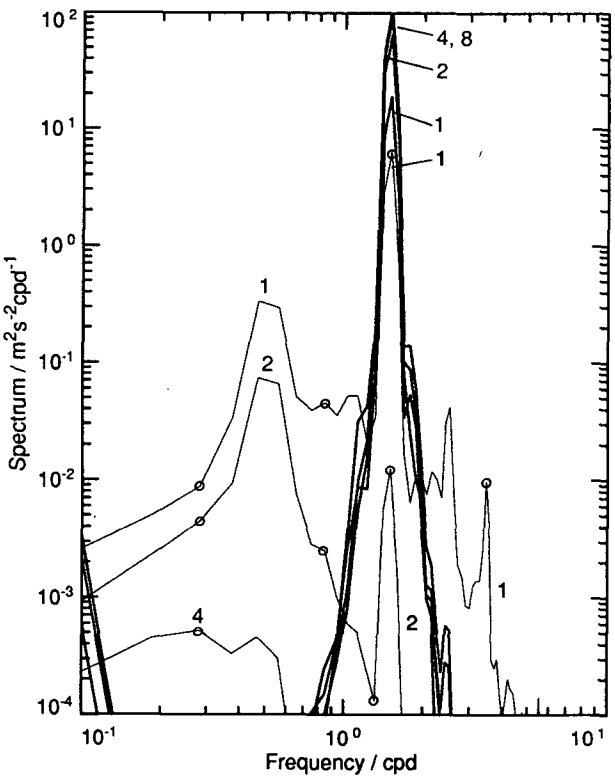

FIG. 3. Spectra of U_L (light curves with circles) and U_I (heavy) demodulated from a pure inertial signal and sampled at Argos fix times. In all cases $fT_I = 4$, while fT_L varies through values 1, 2, 4, and 8 as labeled.

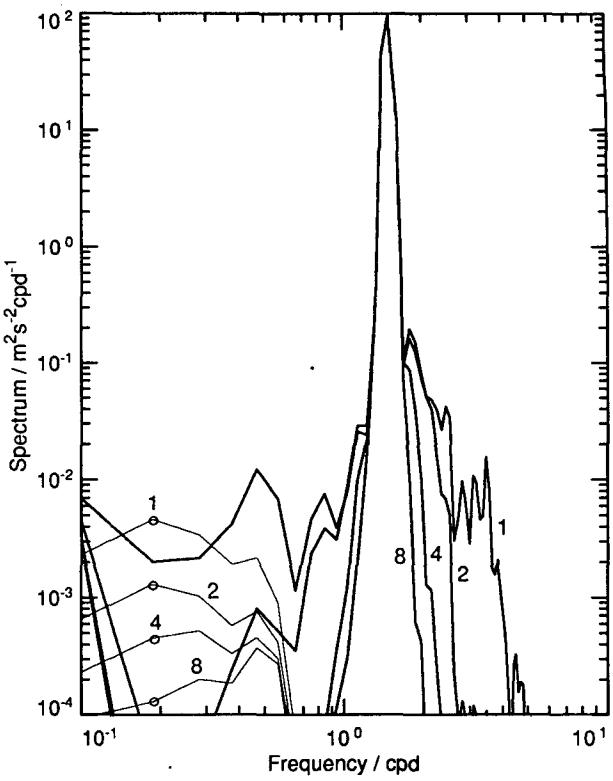

FIG. 4. As in Fig. 3, but $fT_L = 4$, and fT_I varies through values 1, 2, 4, and 8.

$$X_L(t) = S[\mathbf{X}^* - \mathbf{X}_I(\mathbf{t}^*), T_L, \mathbf{t}^*; t]. \quad (6)$$

The difference between X_L and X_{L1} is generally not large.

Low-frequency and inertial velocities are now estimated as

$$U_L(t) = \frac{d}{dt} X_L(t) \quad (7)$$

$$U_I(t) = \frac{d}{dt} X_I(t) \quad (8)$$

with the derivatives computed from the same splines used in (4) and (6). The demodulated inertial velocity is

$$\tilde{U}_I(t) = U_I e^{if t}. \quad (9)$$

The values T_I and T_L were chosen to allow the most rapid variation of $\tilde{U}_I$ and U_L, while adequately suppressing leakage. Figures 3 and 4 show spectra of U_L and U_I for the same pure inertial signal and Argos sampling used in Fig. 2 for various values of T_I and T_L. For a fixed value of $fT_I = 4$ (Fig. 3), a value of fT_L much less than 4 results in a large 0.5-cpd peak, an inertial peak in U_L, and a decrease in the energy in U_I. In particular, for $fT_L = 1$ the 0.5-cpd peak is a factor of 20 worse than in Fig. 2. For a fixed value of $fT_L = 4$ (Fig. 4), a value of fT_I much less than 4

results in large sidelobes in the spectrum of U_I and significant leakage of inertial energy to U_L. The values $fT_I = fT_L = 4$ keep the total spectral leakage below 2×10^{-5}, or less than 0.01 m s^{-1} for a 1 m s^{-1} inertial current. This is about the minimum desirable value. Notice that a small peak in U_L at 0.5 cpd exists in Fig. 4 even for $fT_I = 8$. Larger values of T_I and T_L will suppress this leakage.

An example of the demodulation for a typical OCEAN STORMS drifter is shown for $fT_I = fT_L = 4$ (Fig. 5) and $fT_I = fT_L = 8$ (Fig. 6). The Argos fixes (bottom panel) are visually fit well by the sum of X_I and X_L. In Fig. 5, however, both U_I and U_L ring at a frequency near 0.5 cpd, especially near day 277 where U_I changes rapidly in response to a storm. These fluctuations are highly undesirable if acceleration, for example, is to be computed. The more highly smoothed demodulation in Fig. 6 eliminates this effect at the price of not resolving some real variations in U_L, particularly near day 293, and of spreading the storm generation of inertial currents on day 277 over nearly 3 days. The corresponding spectra (Fig. 7) of U_I (heavy) and U_L (light) show the much cleaner separation of inertial and low-frequency motions for $fT_I = fT_L = 8$. Compared with the velocity spectrum obtained by splining the raw data, ("spline") energy has been eliminated in both the superinertial and 0.5-cpd bands, neither of which is well sampled.

4. Error analysis

The errors in the computed values of $\tilde{U}_I$ and U_L will now be estimated by Monte Carlo simulation of the demodulation process. This provides accurate error estimates and is a robust test of the data analysis programs. The demodulation splits the data $\mathbf{X}^*$ into deterministic parts X_L and X_I and a residual ϵ [Eq. (1)] that is assumed to be a random variable. Additional realizations of $\mathbf{X}^*$, here denoted by $\mathbf{X}_j'$, are generated by

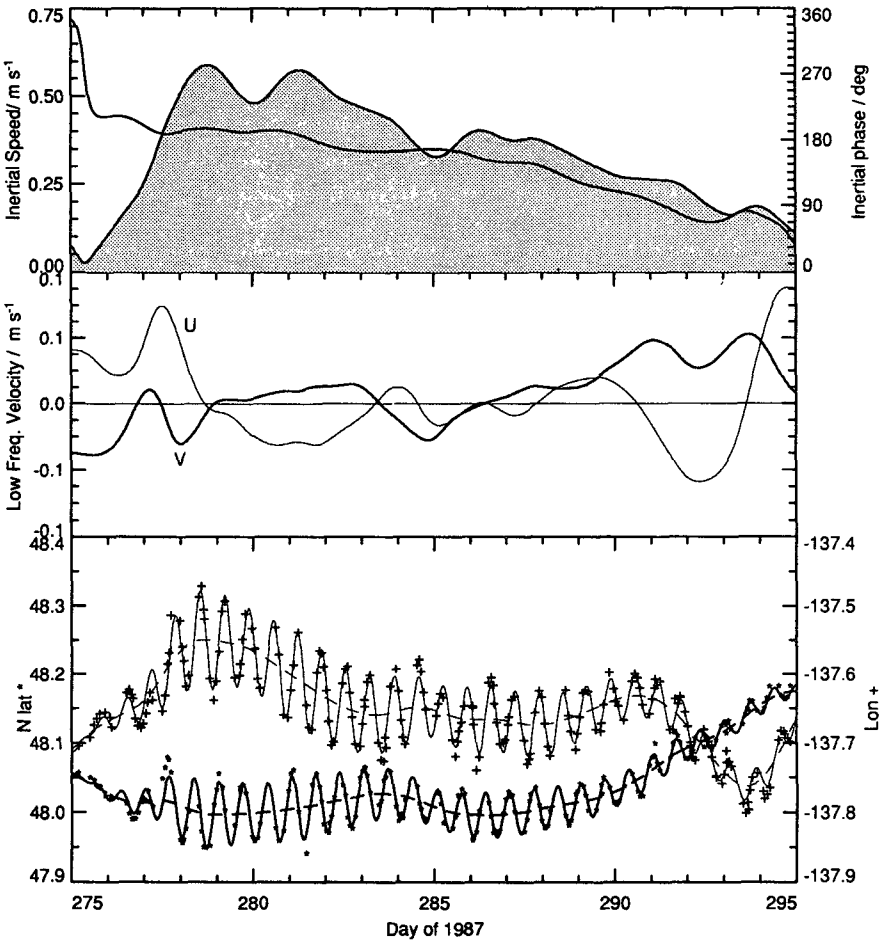

FIG. 5. Demodulation of buoy 7922 for $T_L = T_I = 4/f$. Argos latitude (*) and longitude (+) fixes are plotted in bottom panel. Solid lines through data are the fit; dashed lines are the low-frequency part of the fit. Low-frequency velocity components U_L are plotted in the middle panel. Demodulated inertial velocity $\tilde{U}_I$ is plotted in the top panel as speed (filled) and direction (line).

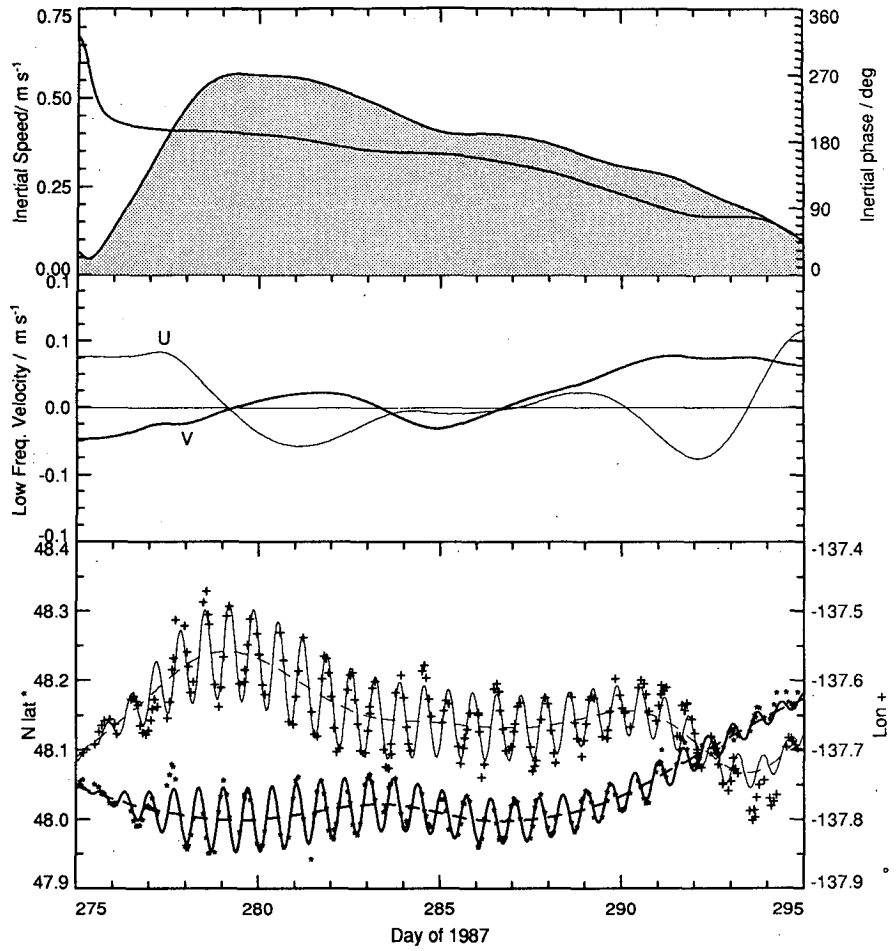

FIG. 6. As in Fig. 5 but for $fT_L = fT_I = 8$.

$$\mathbf{X}'_j(\mathbf{t}^*) = \mathbf{X}_L(\mathbf{t}^*) + \mathbf{X}_I(\mathbf{t}^*) + \sigma_j(\mathbf{t}^*), \quad (10)$$

where X_L and X_I are the deterministic functions of the data and σ_j is the jth realization of a random variable with the same statistical properties as ϵ. Once a suitable model for σ is found, the ensemble of X'_j is used to estimate the errors in the demodulation.

The ϵ can be modeled successfully as the sum of two types of error. First, random errors in the fixes and high-frequency unresolved oceanographic signals are combined into a random position error σ_{Gj}, which is modeled as a Gaussian random variable with a standard deviation of 600 m in each component (for $fT_I = fT_L = 4$). Second, coherent but unresolved subinertial oceanographic velocities are a significant part of the residual. We assume that the oceanic velocity frequency spectrum has a -2 slope and generate a realization of the corresponding displacement:

$$X'_{Cj}(t) = \int_0^t \int_0^{t'} A_C g_j(t) dt dt', \quad (11)$$

where $g_j(t)$ is a random Gaussian variable with zero mean and unit variance, and $A_C = 6 \times 10^{-6}$ m s^{-2} (for $fT_I = fT_L = 4$) is an acceleration that determines the spectral level. Demodulating X'_{Cj} exactly as if it were data yields low-frequency and inertial components X'_{CLj} and X'_{CIj} and a residual

$$\sigma_{Cj} = X'_{Cj} - X'_{CIj} - X'_{CLj}. \quad (12)$$

The model residual

$$\sigma_j = \sigma_{Cj} + \sigma_{Gj} \quad (13)$$

is claimed to have the same statistical properties as ϵ. It is sampled at times

$$\mathbf{t}_j^* = \mathbf{t}^* + \Delta_j, \quad (14)$$

where Δ is a uniform random variable bounded by a maximum absolute value of half a day. This ensures that the results do not depend on the exact timing of the satellite passes.

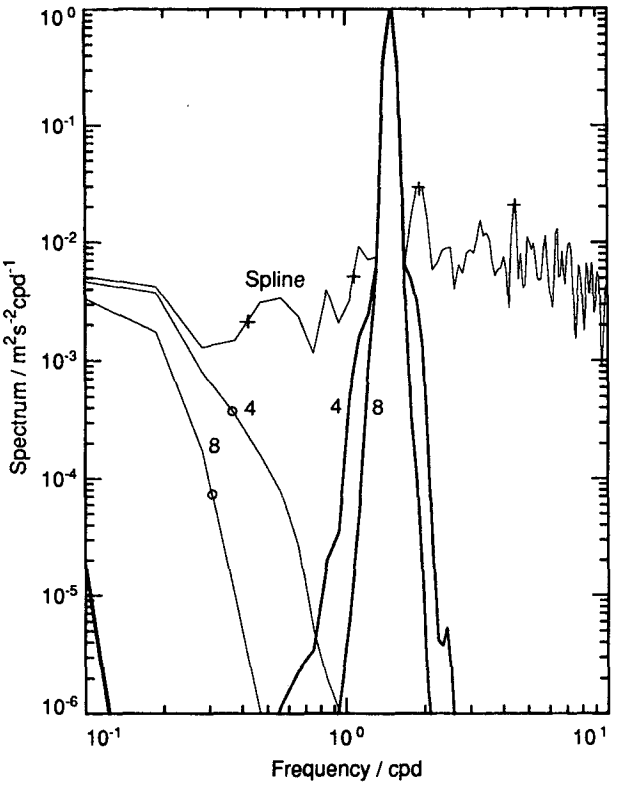

FIG. 7. Spectra of U_I (heavy curves) and U_L (light with circles) from buoy 7922 for $fT_L = fT_I = 4$ and 8. Spectrum of velocity derived from cubic spline of input data is also shown (light with crosses). Spline spectrum follows U_I spectra nearly exactly at f.

Figures 8 and 9 compare the observations and model for $fT_I = fT_L = 4$. The top curve (Fig. 8a) is the spectrum of $\epsilon(t)$, computed by exactly splining the residuals from the demodulation of buoys 7989, 7944, 7985, and 7946 for days 275–300. Below this (Fig. 8b) are 50 realizations of the spectrum, offset one decade downward, of $\sigma_j(t)$ for the same buoys. Figure 9 similarly compares the correlation functions of ϵ (Fig. 9a) and the σ_j (Fig. 9b). Except for a few slightly subinertial points and the semidiurnal frequency, the data, ϵ, are a likely realization of the model, σ. The model form and values of σ_C and σ_G were, of course, varied until this result was achieved. The remaining panels of Figs. 8 and 9 show that a good fit to both the spectrum and the correlation function is obtained only when both components of the error model are included. Using σ_G alone (Figs. 8c and 9c) gives a poor fit to the correlation function, while using σ_C alone (Figs. 8d and 9d) gives a poor fit to the spectrum. Using Δ alone (Figs. 8e and 9e) gives a poor fit to both.

Table 1 shows the estimated errors in U_I and U_L using this error model. The results for 4 buoys differ little from those using 21 (rows 1 and 2). The error in U_I is contributed equally by σ_G and σ_C, while the error in U_L is dominated by σ_C (compare rows 3 and 4). The small error remaining for $\sigma_C = \sigma_G = 0$ (last row) is due to randomly changing the arrival times of the satellites, Δ. The analysis has been repeated for $fT_I = fT_L = 8$. A value of $\sigma_C = 3 \times 10^{-6}$ m s^{-2} now yields the best fit. The errors (Table 1) are smaller.

5. Discussion

The analysis indicates that the inertial and low-frequency components of velocity can be extracted from a perfect oceanographic drifter tracked by Argos at the OCEAN STORMS site with an error of about 0.02 m s^{-1} in each inertial component and 0.008 m s^{-1} in each low-frequency component for a time resolution of about 3 days. Further time averaging will reduce this error. The random component of error that best fits the data is roughly twice that quoted by Argos. This

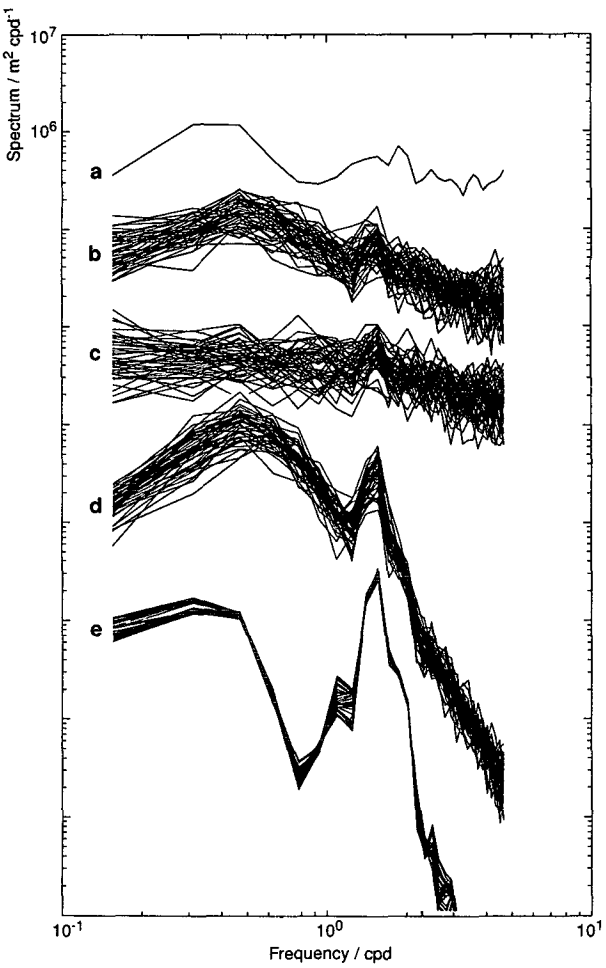

FIG. 8. (a) Spectrum of residual ϵ from demodulation for buoys 7989, 7944, 7985, and 7946 interpolated by cubic spline; $fT_L = fT_I = 4$. (b) 50 realizations of model residual spectra σ for input data from (a). (c) Same as (b), but with $\sigma_C = 0$. (d) Same as (b), but with $\sigma_G = 0$. (e) Same as (b), but with $\sigma_C = \sigma_G = 0$. In (b)–(e), each plot is offset a decade down from the previous one.

may be partially due to unresolved high-frequency surface and internal wave motions of the buoys. The major new results are the large contribution to the error by slightly subinertial motions that are unresolved in the demodulation due to the irregular spacing of the Argos fixes and the multiday smoothing necessary to overcome the effects of the irregular spacing. In regions of higher mesoscale activity, the error contributed by this effect could be significantly larger than found here, particularly for the low-frequency component.

The accuracy of the demodulated inertial currents, about 0.03 m s^{-1} rms, is clearly adequate for resolving inertial currents generated by strong storms, which in OCEAN STORMS exceeded 0.5 m s^{-1}. The frequency constraints imposed by the Argos sampling, however, make it impossible to resolve the details of inertial motion excitation by storms, for example, days 277 and 278 in Figs. 5 and 6, which require a time resolution of a few hours. The accuracy is also marginal for resolving the ambient inertial currents in the mixed layer, which during OCEAN STORMS were generally less than 0.1 m s^{-1}. It may also be marginal for extracting the mixed-layer response to weak storms. The error in the estimated low-frequency velocity is less than that of the inertial and comparable to the drifter error. Longer averaging times will reduce this still further.

TABLE 1. Inertial and low-frequency demodulation errors estimated from the Monte Carlo simulation with 50 realizations. Days 282–299.

Root-mean-square position error (m)	Coherent error A_C (m s^{-2})	Buoys in average	Root-mean-square error east/north (0.01 m s^{-1})	
			Inertial	Low frequency
	$fT_I = fT_L = 4$			
600	6×10^{-6}	21	2.3/2.3	0.78/0.80
600	6×10^{-6}	4	2.3/2.4	0.85/0.78
0	6×10^{-6}	4	1.8/1.8	0.75/0.80
600	0	4	1.6/1.6	0.24/0.24
0	0	4	0.6/0.6	0.08/0.07
	$fT_I = fT_L = 8$			
600	3×10^{-6}	4	1.8/1.8	0.58/0.53

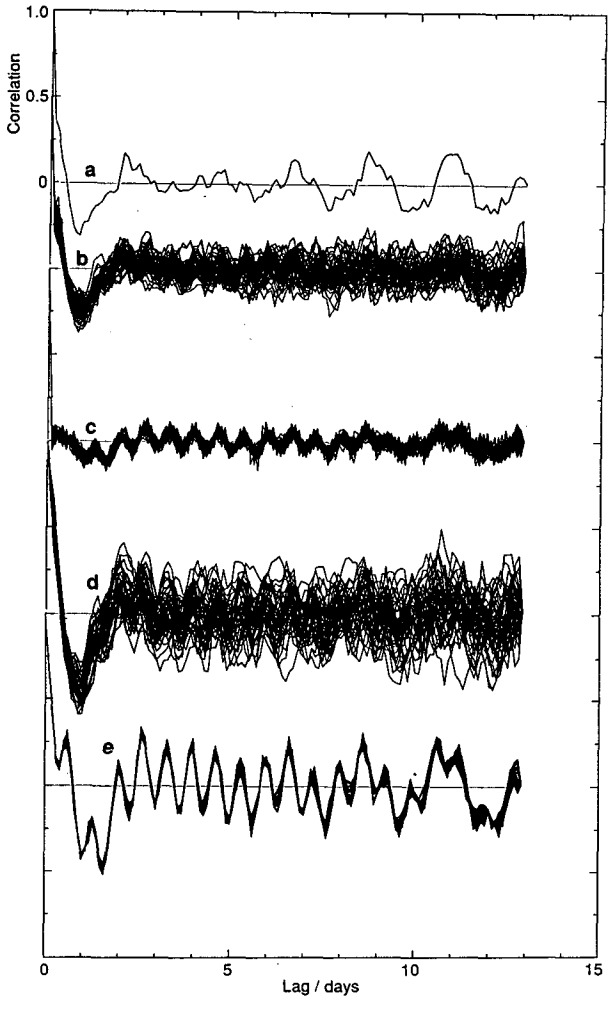

FIG. 9. Same as Fig. 8 but correlation functions.

Given an ideal drifter and perfect tracking, one might hope to infer the stress imparted to the ocean by the wind during a storm, after estimating the mixed-layer depth by some other means. Current Argos tracking is inadequate for resolving the proper time scales.

The Argos sampling at OCEAN STORMS (46°–49°N) is significantly more frequent than at lower latitudes. The leakage effects discussed here will be modified as both the inertial frequency and Argos sampling pattern change with latitude. Nevertheless, the effects of irregular spacing may be subtle, as found here, and the wise should be wary.

Acknowledgments. Peter Niiler was kind enough to allow me to use these data both in real time and after his processing. Brad Bell programmed the spline routines. This work was supported by ONR Contract N00014-87-K-0004 and Grant N00014-90-J-1104. University of Washington School of Oceanography Contribution 1915.

REFERENCES

Chereskin, T. K., P. P. Niiler, and P. M. Poulain, 1989: A numerical study of the effect of upper-ocean shear on flexible drogued drifters. *J. Atmos. Oceanic Technol.*, **6**, 243–253.

Craven, P., and G. Wahba, 1979: Smoothing noisy data with spline functions. *Numer. Math.*, **31**, 377–403.

Niiler, P. P., R. E. Davis, and H. J. White, 1987: Water-following characteristics of a mixed layer drifter. *Deep-Sea Res.*, **34**, 1867–1881.

Poulain, P.-M., 1990: Near inertial and diurnal motions in the trajectories of mixed layer drifters. *J. Mar. Res.*, **48**, 793–823.